

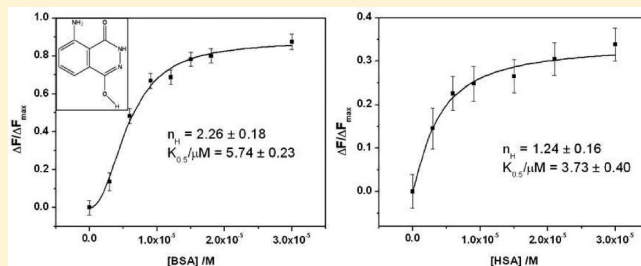
Luminol Fluorescence Quenching in Biomimicking Environments:
Sequestration of Fluorophore in Hydrophobic Domain

N. Shaemningwar Moyon and Sivaprasad Mitra*

Department of Chemistry, North-Eastern Hill University, Shillong 793 022, India

Supporting Information

ABSTRACT: The photophysical behavior of luminol (LH_2) was studied in a variety of biologically relevant systems ranging from surfactants, cyclodextrin, and proteins using steady-state and time-resolved fluorescence spectroscopy. It was shown that, out of two possible LH_2 conformers present in solution, the sequestration of relatively less polar structure into the hydrophobic domain of biological media is the primary reason for decrease in fluorescence intensity. The efficacy of LH_2 fluorescence quenching is substantially higher in micellar subdomain of cationic surfactant and depends on the nature of the head-group. The thermodynamic parameters like enthalpy (ΔH) and entropy (ΔS) change, etc., corresponding to the binding of LH_2 in the model water-soluble protein, bovine serum albumin (BSA), were estimated by performing the fluorescence titration experiment at different temperatures. The involvement of subdomain IA and IIA of BSA in LH_2 binding was confirmed from the ligand replacement process with bilirubin (BIL). The difference in ligand binding with structurally homologous human serum albumin (HSA) is discussed in terms of positive cooperativity among these two binding domains of BSA with a Hill coefficient (n_H) value of 2.26 ± 0.18 and a half-maximal concentration ($K_{0.5}$) of $5.74 \pm 0.23 \mu\text{M}$ at 298 K.



1. INTRODUCTION

Luminol (3-aminophthalic hydrazide, LH_2) is being extensively used in recent times by forensic investigators as a tool to detect trace blood patterns in a crime scene and applied as an aerosol in a mixture with sodium perborate, sodium carbonate, and distilled water.^{1,2} LH_2 is known to possess a striking blue chemiluminescence when mixed with an appropriate oxidizing agent. This unique deep blue chemiluminescent glow enables it to be used as an assay to detect several species like metal ions, hydrogen peroxide, nitrate, some alcohols, amines, amino acids, carbohydrates, cyanides, enzyme and enzyme substrates, and also vitamins.^{3–7} Further, LH_2 -enhanced chemiluminescent probes have also been used to characterize and quantify the secretion of oxygen by phagocytosing cells.⁸ Although there is no evidence of LH_2 being currently used as a therapeutic agent, early clinical setting evidence for the use of LH_2 in the treatment of fluid accumulation of tissues in critically ill patients⁹ as well as patches of baldness caused by autoimmune disease alopecia¹⁰ and promotory activity in blood clotting and wound healing is also found in the literature.^{11,12} Nowadays, LH_2 reactions in water have been intensely investigated due to its importance in forensic applications.

Fluorescence is similar to chemiluminescence, the only exception being the excitation source (a light source being used to excite the electrons in the former instead of an appropriate chemical reaction in the later). Thus, one can monitor the variation in LH_2 fluorescence intensity to understand its interaction with several biochemical environments. Also, the fluorescence properties of

LH_2 have been successfully applied in different analytical and biochemical applications.^{13–16}

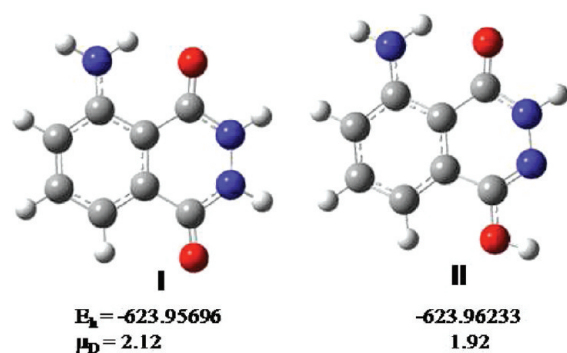
Recently, we investigated the fluorescence emission behavior of LH_2 in a variety of solvent media and also performed a detail density functional theory calculation on several possible isomeric structures of LH_2 under different degrees of hydration.¹⁷ The main conclusions obtained are as follows: (a) the fluorescence spectral position shows appreciable red shift along with almost 2-fold increase in yield (ϕ_f) in polar protic solvents in comparison with the apolar counterpart; (b) hydrogen bond donation ability (α) of the solvent is the primary parameter controlling the excited-state behavior of LH_2 ; and (c) out of several possible tautomeric forms, only the structures represented by **I** and **II** (Chart 1) are the principal contributors toward the photoluminescence behavior of LH_2 . Further, in a separate communication, interaction of LH_2 with human serum albumin (HSA) was also reported.¹⁸ Serum albumins are known to be the major soluble protein constituents of the circulatory system and have many physiological functions.^{19,20} The most important property of this group of proteins is that they can serve both as depot protein as well as transport protein for a variety of exogenous compounds.²¹ As a result, chemiluminescence behavior of LH_2 is being extensively used to quantitatively detect several proteins and cancer biomarkers by a variety of techniques.^{5–7} However, to be used as

Received: May 12, 2011

Revised: June 20, 2011

Published: June 30, 2011

Chart 1. Fully Optimized Structure of the Most Important Isomeric Form of LH₂ along with the Corresponding Gas-Phase Energy (E) and Dipole Moment (μ) Obtained by B3LYP/6-311++G(d,p) Calculation



an efficient biomarker assay, it is indispensable to study the fluorescence properties of LH₂ in the presence of other biologically relevant media like surfactants, cyclodextrin, etc. In the present paper, we further elaborate on this venture and report the finding of LH₂ fluorescence behavior in several biomimicking environments like surfactant and cyclodextrin as well as other carrier protein, bovine serum albumin (BSA). Common surfactants with cationic, anionic, and neutral head groups like cetyltrimethylammonium bromide (CTAB), sodium dodecyl sulfate (SDS), and TritonX-100 (TX-100), respectively, and β -cyclodextrin (CD) are used as biomimicking environments. Also, detailed investigation results of LH₂ interaction with BSA are reported along with the differences in thermodynamic parameters and binding mode with structurally homologue HSA.

2. MATERIALS AND METHODS

2.1. Chemicals. Luminol (LH₂, 97%) was received from Sigma-Aldrich Chemical Pvt. Ltd. (product no. 123072) and used without any further purification. The analytical grade type II water, used as solvent, was obtained from Elix 10 water purification system (Millipore India Pvt. Ltd.). The samples were dissolved in Tris-HCl buffer solution (0.05 mol dm⁻³ Tris and 0.15 mol dm⁻³ NaCl, pH = 7.4 \pm 0.1). β -Cyclodextrin (CD) was obtained from Aldrich Chemical Co., whereas spectroscopic grade 1,4-dioxane and the surfactants sodium dodecyl sulfate (SDS), cetyltrimethylammonium bromide (CTAB), and TritonX-100 (TX-100) were procured from Sigma-Aldrich (India) and all were used as received. Essentially fatty acid and globulin free, $\geq 99\%$ (agarose gel electrophoresis), lyophilized powder form of bovine serum albumin (BSA, Sigma, cat. no. B4287) and human serum albumin (HSA, USB Corp. USA, cat. no. 10878) were used as received. The buffer Tris had a purity of no less than 99.5%, whereas analytical grade NaCl, HCl, and bilirubin (BIL) were all obtained from Sisco Research Laboratory (SRL), India. The solution pH was checked with Systronics μ -pH system 361. The chromophore concentration ($\sim 5 \mu\text{M}$) was very low to avoid any aggregation and/or contribution toward primary or secondary inner filter effects. The sample concentration was kept constant during several additions of different microheterogeneous medium. All the solutions were prepared afresh and kept for about half an hour for settling before the spectroscopic measurement.

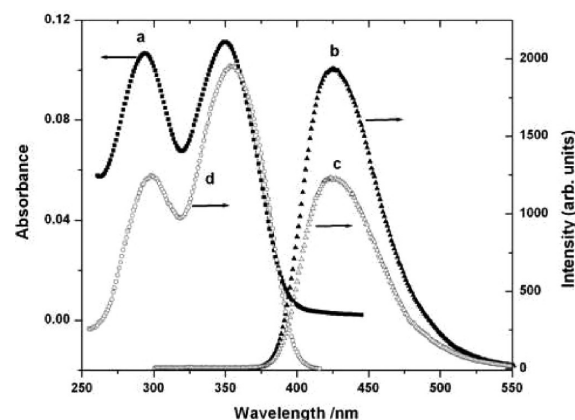


Figure 1. Steady-state absorption (a), fluorescence emission (b and c with $\lambda_{\text{exc}} = 360$ and 290 nm, respectively) excitation (d, $\lambda_{\text{mon}} = 425$ nm) spectra of $\sim 5.0 \mu\text{M}$ LH₂ solution in buffer of pH = 7.4.

2.2. Experimental Procedure and Data Analysis. Steady-state absorption spectra were recorded on a Perkin-Elmer model Lambda25 absorption spectrophotometer. Fluorescence spectra were taken in a Hitachi model FL4500 spectrofluorimeter and all the spectra were corrected for the instrument response function. Quartz cuvettes of 10 mm optical path length received from PerkinElmer, USA (part no. B0831009) and Hellma, Germany (type 111-QS) were used for measuring absorption and fluorescence spectra, respectively. For fluorescence emission, the sample was excited at 360 nm unless otherwise mentioned, whereas excitation spectra were obtained by monitoring at the respective emission maximum. In all cases, 5 nm bandpass was used in the excitation and emission side. Any possible contribution of inner filter effect due to attenuation of the incident light by the quencher is negligible, since none of the components providing the biomimicking environment have any significant absorption at the excitation wavelength. Nevertheless, each fluorescence spectrum (F) of LH₂ in the presence of different concentrations of the additives was corrected for any possible inner filter effect using the following equation²²

$$F^{\text{corr}}(\lambda_E, \lambda_F) = F(\lambda_E, \lambda_F) \times \frac{A(\lambda_E)}{A_{\text{tot}}(\lambda_E)} \quad (1)$$

where A represents the absorbance of the free LH₂ and A_{tot} is the total absorbance of the solution at the excitation wavelength (λ_E). The corrected spectrum can be taken as the only LH₂ contribution toward fluorescence. All steady-state data obtained from three separate experiments were averaged and further analyzed using Origin 6.0 (Microcal Software, Inc., USA). Fluorescence quantum yields (ϕ_f) were calculated by comparing the total fluorescence intensity under the whole fluorescence spectral range with that of a standard (quinine bisulfate in 0.5 M H₂SO₄ solution, $\phi_f^s = 0.546$ ²³) with the following equation using adequate correction for solvent refractive index (n).²⁴

$$\phi_f^i = \phi_f^s \times \frac{F^i}{F^s} \times \frac{(1 - 10^{-A^s})}{(1 - 10^{-A^i})} \times \left(\frac{n^i}{n^s} \right)^2 \quad (2)$$

where A^i and A^s are the optical density of the sample and standard, respectively, and n^i is the refractive index of solvent at 293 K. The relative experimental error of the measured quantum yield was estimated within $\pm 5\%$. The temperature

variation experiments were carried out by attaching a circulatory thermostat bath (MLW, Germany, type U2C) to the cell holder.

Fluorescence decay analysis were performed using time-correlated single photon counting (TCSPC) technique as implemented in the time-resolved spectrofluorimeter FL-920 (Edinburg Instruments, UK). The samples were excited at 375 nm and emission was collected with magic angle configuration at the respective fluorescence peak position using 4096 channels with 100 ns time window. The sample fluorescence was analyzed with nonlinear iterative deconvolution method based on Marquardt algorithm using sum of exponential decay with baseline correction function.²⁵

3. RESULTS AND DISCUSSION

3.1. Steady-State Spectral Properties in Homogeneous Media. Figure 1 represents the steady-state spectral properties of LH₂ in aqueous buffer solution of pH = 7.4. It is observed that LH₂ possesses two distinct absorption bands. One high-energy peak appears at the 280–320 nm region, whereas the other low-energy absorption in the 330–380 nm region. However, the emission obtained by exciting at both these absorptions shows strongly intense, unstructured and broad spectra ranging from 375 to 520 nm. The excitation spectra corresponding to this emission closely resembles the absorption profile. As discussed in our previous publication,¹⁷ the origin of the broad absorption in the 330–380 nm region can be assigned as $S_1(\pi) \leftarrow S_0(\pi)$ transition, whereas the origin of the high energy absorption at ~ 300 nm may be due to $S_2(\pi) \leftarrow S_0(\pi)$ excitation. Before going into the details of the fluorescence properties in the micellar environment, it is worth discussing the behavior of the probe in the homogeneous mixture of water and 1,4-dioxane, as these mixtures are known to mimic the micellar environment very closely.²⁶ With increasing volume fraction of water in 1,4-dioxane, both the fluorescence spectral position and intensity shift regularly and finally show about 30 nm red shift along with almost 3 times increase in fluorescence quantum yield (ϕ_f) in pure aqueous medium. Representative fluorescence emission spectral profiles along with the corresponding data are shown in Figure 2a. However, the fluorescence excitation spectra (Figure 2b) do not show any major change while going from 1,4-dioxane to water, the only exception being the loss of vibrational structure in the high-energy band accompanied by a little broadening of the 350 nm peak. As reported in our earlier publication, this difference in fluorescence properties in aqueous media is due to the stabilization of the excited state through formation of specific hydrogen bond of LH₂ with water.¹⁷ The hydrogen bond formation occurs through the solvent hydrogen bond donation property toward the electron-rich charge-localized centers like imine nitrogen and carbonyl oxygen of the 2- and 4-positions of the phthalhydrazide ring system of LH₂. The most important isomeric structures responsible for LH₂ fluorescence behavior are shown in Chart 1 along with some of the calculated parameters using B3LYP/6-311++G(d,p) formalism. Very small energy differences among different hydrogen-bonded clusters of I and II as well as possible dynamic interconversion among them may contribute toward the broad nature of LH₂ spectral profiles, particularly in a protic solvent like water.

3.2. Steady-State Spectral Properties in Micellar Media. The absorption maximum for the aqueous solution of LH₂ is practically unaffected by the presence of added surfactant, indicating very low absorbance sensitivity to the changes in

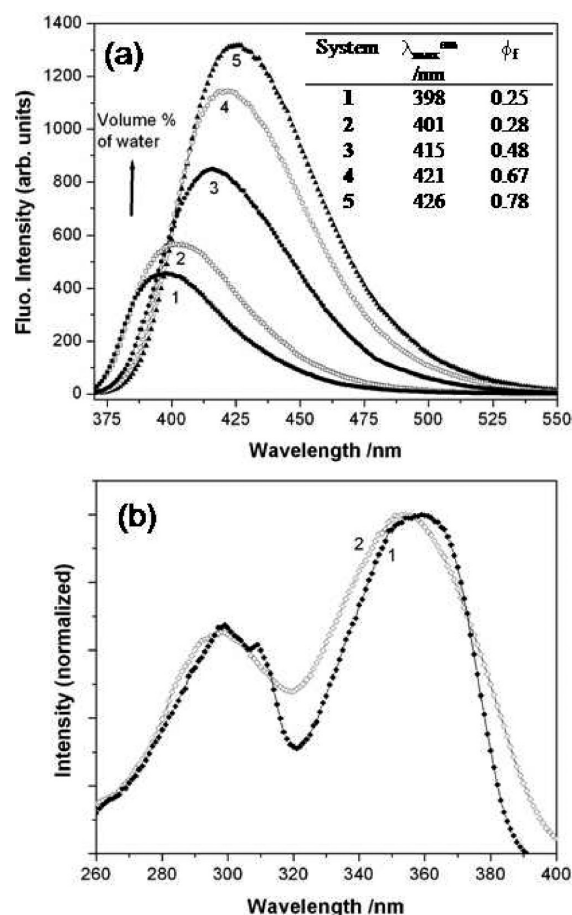


Figure 2. Steady-state fluorescence emission (a) and excitation (b) spectra of LH₂ in varying water/1,4-dioxane content. (a) Volume percent of water = 0 (1), 10 (2), 50 (3), 75 (4), and 100 (5). Inset shows the fluorescence emission maxima ($\lambda_{\text{max}}^{\text{em}}$) and quantum yield (ϕ_f) in different systems. (b) 1,4-Dioxane (1) and water (2).

surfactant concentration. However, the intensity of the fluorescence spectrum changes with the amount of surfactant in solution. Gradual addition of all the surfactants (CTAB, TX-100, and SDS) is associated with an initial increase within very small surfactant concentration followed by steady decrease in LH₂ fluorescence intensity. Figure 3 shows some representative spectral profiles along with the pattern of intensity variation in each case. The increase in fluorescence intensity at very low surfactant concentration is due to the increased solubility of the organic fluorophore; however, it is clear that the fluorescence intensity decreases continuously after a certain concentration of surfactant in the solution, which is quite close to the critical micelle concentration (cmc) of the individual surfactant system. Once the micellar structure is formed, the fluorophore is partitioned in the hydrophobic micellar pseudophase from the bulk aqueous medium. As a result, the average steady-state fluorescence intensity of the solution would decrease, which is consistent with the observations made above for homogeneous solvents like water buffer and 1,4-dioxane. Interestingly, it is evident from the inset of Figure 3, a and c, that the rate at which intensity decreases after the micelle formation is relatively higher in the case of the cationic micellar system CTAB in comparison with anionic SDS. However, it is rather difficult to quantitatively compare the TX-100 data given in the inset of Figure 3b as the

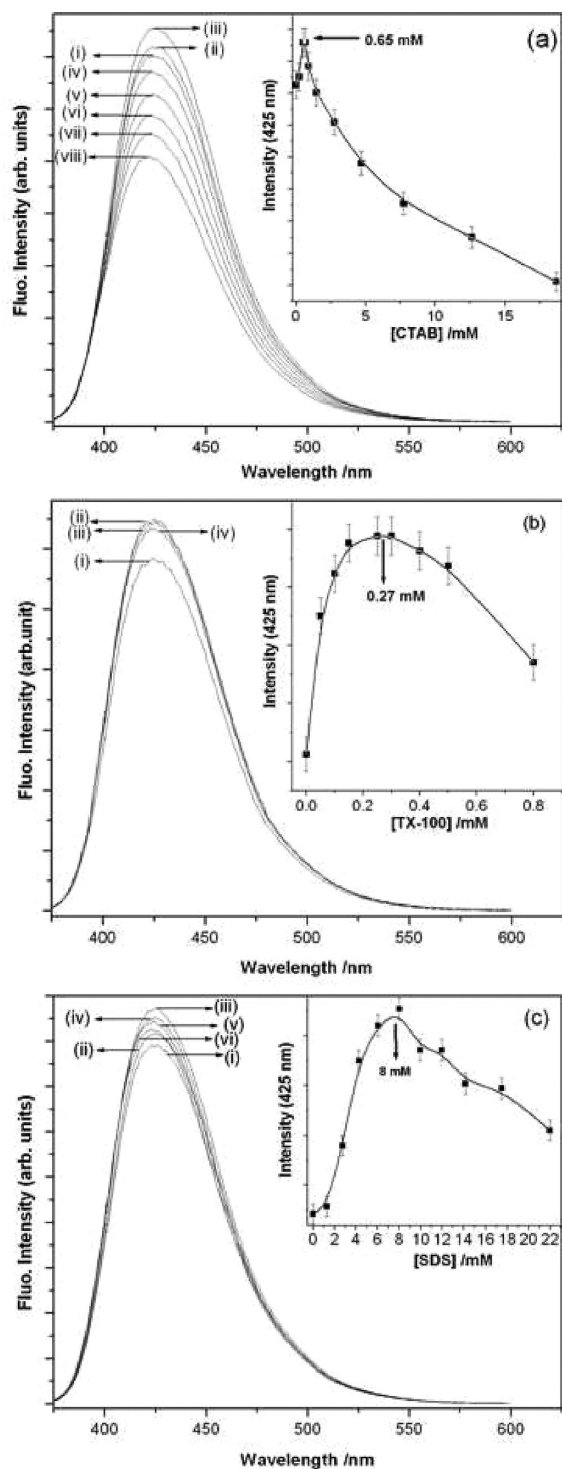


Figure 3. Change in LH₂ fluorescence emission profile ($\lambda_{\text{exc}} = 360$ nm) with increasing concentration of CTAB (a), TX-100 (b), and SDS (c). The concentration of the surfactants are (a) [CTAB]/mM = 0.0 (i), 0.5 (ii), 1.4 (iii), 2.7 (iv), 4.7 (v), 7.8 (vi), 12.5 (vii), and 18.7 (viii); (b) [TX-100]/mM = 0.0 (i), 0.25 (ii), 0.30 (iii), 0.5 and (iv); and (c) [SDS]/mM = 0.0 (i), 2.7 (ii), 8.0 (iii), 11.9 (iv), 12.5 (v), and 21.9 (vi). Inset shows the variation in fluorescence intensity at 425 nm in each case.

concentration range used in this case is at least an order of magnitude lower than the other two. Apparently, the fluorescence peak position is not too sensitive toward the micellar medium.

However, careful analyses of the data presented in Table 1 as well as Figure 3 reveal that fluorescence spectral blue shift is somewhat greater in the case of interaction with CTAB (~ 3 nm) in comparison with the other surfactant systems. In analogy with the results discussed above for water/1,4-dioxane solvent mixture, a blue shift of the fluorescence maximum suggests that the polarities of the micellar environments are less than the polarity of the bulk water. However, the fluorescence maxima of LH₂ in fully micellized condition (Table 1) indicate that the probe is not incorporated into the core; rather, it stays more or less in the interfacial region of the micelle. Nevertheless, the data presented in Table 1 indicates stronger interaction of LH₂ with CTAB. The decrease in LH₂ fluorescence intensity in micellar medium can be rationalized on the basis of the passage of the relatively nonpolar fluorophore (structure II, Chart 1) toward more hydrophobic interfacial region. However, due to extensive charge localization in the excited state,¹⁷ LH₂ interacts more strongly with a cationic micelle like CTAB. The presence of this dipole–dipole type of interaction in addition to the hydrophobic force causes much stronger interaction with CTAB in comparison with other surfactant systems as evidenced by (a) a rapid fall in fluorescence intensity and also (b) detectable blue shift in fluorescence spectral position. This point is further confirmed from the time-resolved studies as well as thermodynamics of ligand binding in BSA discussed below. Similar results were reported recently for the fluorescence behavior of 8-hydroxypyrene-1,3,6-trisulfonate, trisodium salt (HPTS).²⁷ It was shown that the extent of excited-state deprotonation and quenching of neutral and/or anionic fluorescence of HPTS is drastically different and depends strongly on the nature (cationic, anionic, or neutral) of the surfactant. It is to be noted here that, while discussing the principle driving force and the stability of LH₂–micelle complex in different surfactant systems, neither the dimension of the micelle nor the aggregation number was taken into consideration. However, a rigorous description of the forces responsible for binding the chromophore in the micellar subdomain should involve the size of the respective micelles and its change with increasing surfactant concentration as well as the spatial distribution of the fluorophore in the interfacial region. Nevertheless, a qualitative description based on the averaged parameters of the probe as well as the micellar system is reasonable, given the tendency of the hydrophobic environments to quench LH₂ fluorescence and also the time-dependent fluorescence decay behavior in different media discussed in the following section.

3.3. Time-Resolved Fluorescence Behavior. Picosecond time-resolved fluorescence decay measurement of LH₂ emission in homogeneous buffer solution indicates a biexponential decay function with corresponding decay time of 2.4 ns (24%) and 9.8 ns (76%). In analogy with our earlier report, the short and long decay time component of LH₂ fluorescence can be assigned to structures I and II, respectively.¹⁸ The fluorescence decay behavior was also monitored in the presence of added surfactants. All the experimental decay curves could be well reproduced again with two-exponential decay functions as evidenced by the statistical parameters like reduced chi-square (χ^2) and distribution of weighted residuals. Figure 4 shows some representative decay profiles in varying concentrations of CTAB along with the fitting data, and Table 1 collects all the relevant data for different surfactants. From the table, it is clear that the fluorescence decay time of the two components remains practically unaffected in the presence of all the surfactants. The relative contribution of the first decay component increases in the presence of all the

Table 1. Fluorescence Spectral Behavior of LH₂ ($\sim 5 \mu\text{M}$) in Homogeneous Buffer Solution and in Different Heterogeneous Media^a

medium		$\lambda_{\text{max}}^{\text{em}}$ (nm)	ϕ_{f}	decay parameters			χ^2
				τ_1/ps (α_1)	τ_2/ns (α_3)	τ_3/ns (α_3)	
buffer (pH = 7.4)		426	0.78	—	2.4 (0.24)	9.8 (0.76)	1.19
CTAB	0.5 mM	426	0.84	—	2.5 (0.24)	9.9 (0.76)	1.12
	12.5 mM	423	0.61	—	2.4 (0.61)	9.5 (0.39)	1.14
TX-100	0.15 mM	426	0.89	—	2.3 (0.25)	9.7 (0.75)	1.20
	0.6 mM	426	0.77	—	2.4 (0.36)	9.6 (0.64)	1.15
SDS	2.4 mM	426	0.81	—	2.4 (0.24)	9.9 (0.76)	1.15
	20 mM	426	0.59	—	2.5 (0.34)	9.5 (0.66)	1.20
BSA	6 μM	423	0.30	<100 (0.65)	1.8 (0.12)	8.9 (0.23)	1.02
	30 μM	420	0.11	<100 (0.60)	1.0 (0.27)	8.8 (0.13)	1.2
HSA	6 μM	426	0.62	<100 (0.71)	2.0 (0.08)	9.0 (0.21)	1.10
	30 μM	426	0.53	<100 (0.73)	1.6 (0.09)	9.0 (0.18)	1.12

^a The preexponential factor and the decay time are represented by α and τ , respectively; the relative error in measuring τ values is within ± 0.1 ns.

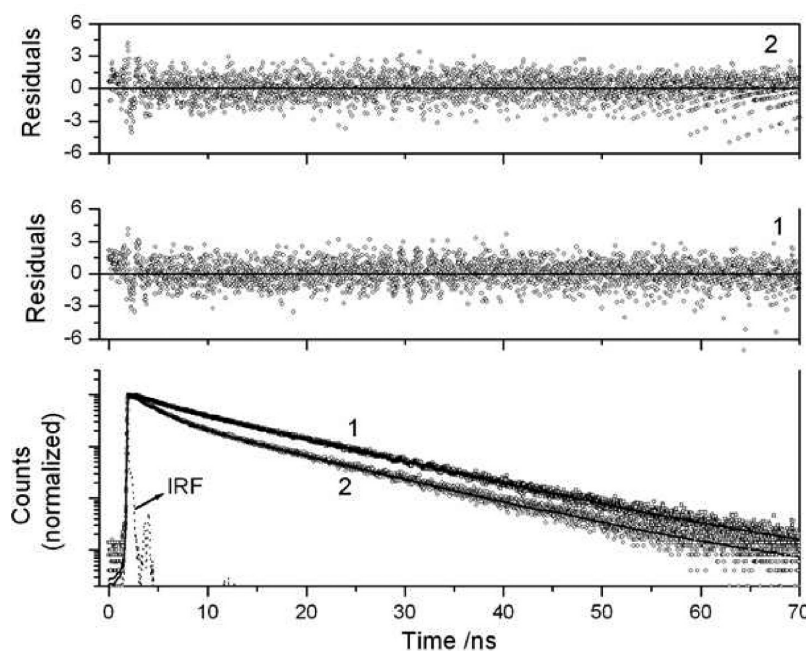


Figure 4. Time-resolved fluorescence decay profile (open circles) of aqueous LH₂ in the presence of varying concentrations of CTAB along with the simulated data (solid lines). [CTAB]/mM = 0.5 (1) and 12.5 (2), respectively. The upper panels show the distribution of weighted residuals for two-exponential fitting in each case. IRF indicates the instrument response function.

surfactant concentrations above cmc. However, in the case of CTAB, this increase is almost $2^{1/2}$ times in comparison with that of the bulk aqueous medium. This observation further supports the idea of relatively stronger interaction in CTAB micelles as discussed before.

3.4. Fluorescence Behavior in β -Cyclodextrin (CD) and Mixed CD–Surfactant System. The unique property of cyclodextrin (CD) to encapsulate organic compounds inside its hydrophobic central cavity make them potential candidate as extremely efficient molecular vehicles for drug delivery.²⁸ Furthermore, the reduced polarity and restricted geometry of the interior cyclodextrin cavities gives an opportunity to study different photophysical properties in tailored environmental conditions. The inclusion of the organic probe is primarily

controlled by the size fitting of the host toward the guest cavity.²⁹ The LH₂ fluorescence intensity seems to increase moderately on addition of CD until it reaches a plateau along with a spectral blue shift of about 5 nm (Figure 5a). As seen in the previous section about the LH₂ fluorescence quenching in micellar medium, it is rather surprising to observe an enhancement in fluorescence intensity on binding with the hydrophobic CD cavity. In fact, little increase in molecular fluorescence of LH₂ derivatives in presence of CD was reported as early as in mideighties; however, no possible explanation was given for that.³⁰ Recently, Maeztu et al. also reported the enhancement of chemiluminescence intensity of LH₂ and its derivatives at alkaline pH in presence of natural cyclodextrins.^{31,32} In addition to the size requirement for the entire or partial inclusion of the guest molecule inside the

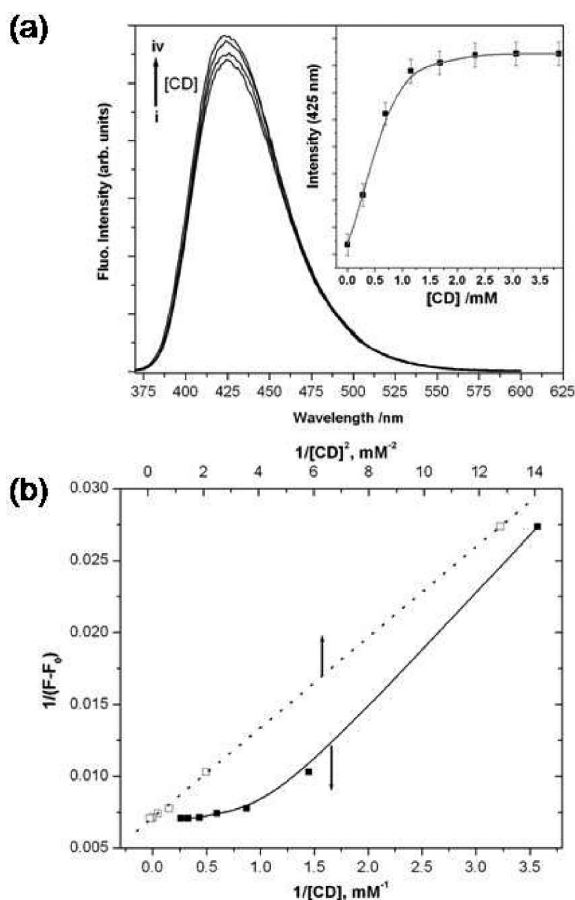


Figure 5. (a) Variation of LH₂ fluorescence spectral profile on addition of β -cyclodextrin (CD). [CD] /mM = 0 (i), 0.3 (ii), 0.7 (iii) and 3.8 (iv). Inset shows the intensity variation at 425 nm. (b) Double reciprocal plot for 1:1 (solid line) and 2:1 (dotted line) of the CD-LH₂ complex obtained from eqs 3 and 4.

CD cavity, additional hydrophobic forces are also important in determining the geometry of the complex.^{33,34} Nevertheless, an increase in LH₂ fluorescence intensity in presence of CD can stem from the fact that considers the restricted nonradiative motion, and thereby reducing the vibrational deactivation of the caged analyte.

The apparent binding constant and stoichiometric ratio of the inclusion complex can be determined from the modified Benesi-Hilderbrand (BH) equation using the fluorescence data. The equations can be written in the following forms for the formation of 1:1 and 1:2 guest–host complexes, respectively:³⁵

$$\frac{1}{F - F_0} = \frac{1}{F_\infty - F_0} + \frac{1}{K_{a1}(F_\infty - F_0)} \times \frac{1}{[CD]} \quad (3)$$

$$\frac{1}{F - F_0} = \frac{1}{F_\infty - F_0} + \frac{1}{K_{a2}(F_\infty - F_0)} \times \frac{1}{[CD]^2} \quad (4)$$

where F_0 and F are LH₂ fluorescence intensities in absence and presence of CD, respectively. F_∞ indicates the fluorophore intensity at the plateau and K_a indicates the association constant in the respective cases. Figure 5b shows the double reciprocal plot for the LH₂–CD system. The linearity for the 1:2 case indicates that LH₂ is bound with two CD molecules and the binding constant is calculated to be $4.2 \times 10^6 \text{ M}^{-2}$ from the slope

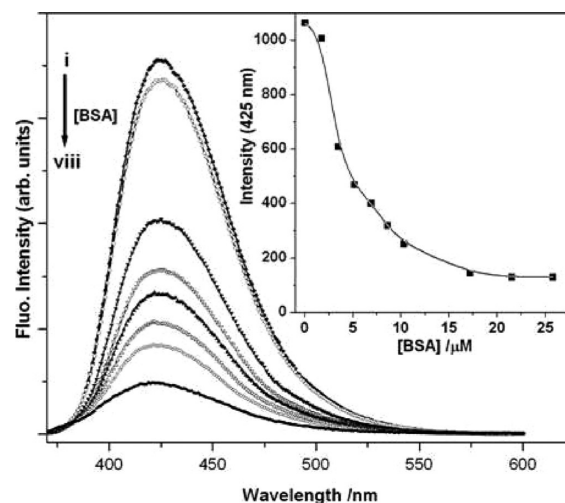


Figure 6. Variation of LH₂ fluorescence spectral profile on addition of bovine serum albumin (BSA). [BSA] / μM = 0 (i), 1.7 (ii), 3.5 (iii), 5.1 (iv), 6.9 (v), 8.6 (vi), 10.3 (vii), and 17.2 (viii). Inset shows the intensity variation at 425 nm.

and intercept of the simulated data. Interestingly, the fluorescence intensity is also found to increase upon gradual addition of CD in LH₂ solution containing a fixed amount (12.5 mM) of CTAB (Figure 1S in the Supporting Information). However, the BH plot in this case indicates a complex with 1:1 stoichiometry with an apparent binding constant of 101.4 M^{-1} (inset, Figure 1S). This difference in stoichiometry may be due to the fact that the nature and intensity of the feeble forces responsible for the formation of the complex change in the presence of an ionic micellar medium like CTAB.

3.5. Interaction of LH₂ with Serum Albumins. The fluorescence intensity of LH₂ decreases regularly with the increasing concentration of BSA accompanied by about 10 nm blue shift in the emission maximum. Figure 6 shows the representative emission spectral profile in the presence of various concentrations of BSA. The rapid quenching of LH₂ fluorescence indicates a strong interaction of LH₂ with BSA. In the inset of Figure 6, the fluorescence intensity was plotted against the quencher concentration. Interestingly, the decrease in intensity shows a clear sigmoidal shape. It is to be noted here that the LH₂ fluorescence intensity was also found to decrease with HSA concentration;¹⁸ however, the nature of fluorescence intensity decrease is non-sigmoidal (inset of Figure 2S in the Supporting Information). The decrease in LH₂ fluorescence intensity can be assumed again as the passage of the probe molecule from the aqueous bulk phase and binding toward a more hydrophobic region in the ligand binding domain of the proteins. Binding of LH₂ in albumin is further reinforced by a ligand replacement process in the presence of bilirubin (BIL). On subsequent addition of BIL to an LH₂/BSA solution, the fluorescence intensity of LH₂ is recovered (Figure 3S in the Supporting Information). BIL is known to have very strong affinity toward the albumins and binds in the ligand binding domains with apparent binding constant varying within the range of approximately 10^6 – 10^8 M^{-1} .³⁶ This value is higher by almost 3 orders of magnitude compared to that in the case of LH₂ in BSA (see below). With the preferential incorporation of BIL into the ligand binding site, the bound LH₂ is expelled in the more aqueous phase; consequently, the fluorescence intensity increases. Interestingly, this recovery of fluorescence in the presence of BIL can be

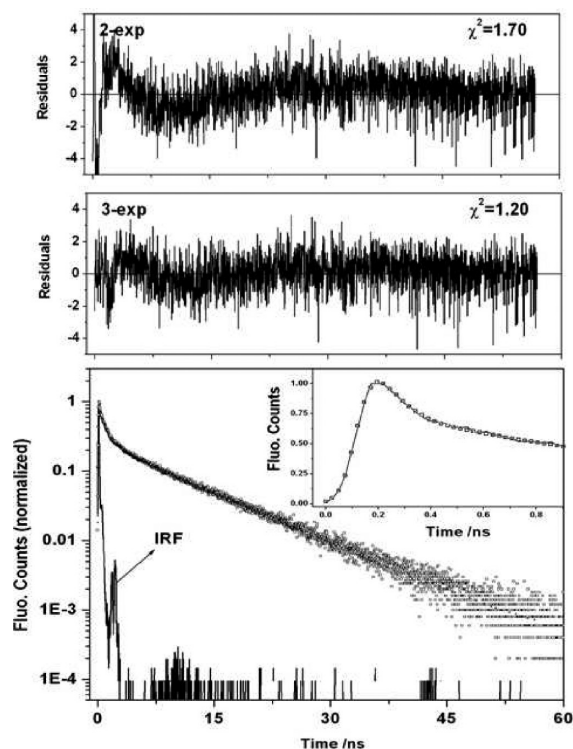


Figure 7. Fluorescence decay profile (open circles) and simulated data (solid line) with three-exponential decay function of LH_2 in presence of 30 μM BSA. $\lambda_{\text{exc}} = 375$ nm and $\lambda_{\text{mon}} = 430$ nm. IRF indicates the instrument response function. Inset shows the same data in shorter time scale. Upper panels show the distribution of weighted residuals and χ^2 values obtained from the fitting of the experimental data using three-exponential (3-exp) and two-exponential (2-exp) decay models, respectively.

explored in further detail and used as an assay for efficient application of LH_2 for analytical and/or forensic purposes.

The fluorescence decay behavior of LH_2 in the presence of BSA is markedly different from what is observed in homogeneous buffer and also the micellar medium (Table 1). Although the decay time corresponding to species I and II is still found to be ~ 2 and ~ 9 ns, respectively, a major portion (ca. 65%) of the excited fluorophore decays with very short instrument-limited lifetime (< 100 ps). The presence of the first decay component in the presence of BSA is obvious from Figure 7. Furthermore, a comparison of the statistical parameters like reduced χ^2 values as well as visual inspection of the weighted residuals confirm that two-exponential fitting of the experimental data is insufficient and a minimum of three-exponential decay function is necessary. In contrast, no such fast decay was observed for LH_2 in the presence of other heterogeneous micellar media as discussed earlier and also shown in Table 1. Similar observation was also made in the presence of HSA and explained on the basis of the formation of closely spaced fluorophore–quencher pair, where the fluorescence is quenched rapidly in the presence of the quencher and appears to be dark under this experimental condition.¹⁸

3.5.1. Stern–Volmer Analysis of Fluorescence Quenching Data. The fluorescence quenching data are usually analyzed by the Stern–Volmer (SV) equation

$$\frac{F_0}{F} = 1 + \kappa_q \tau_0 [Q] = 1 + K_{SV} [Q] \quad (5)$$

where F_0 and F are the fluorophore intensities in the absence and presence of quencher, respectively. K_{SV} , κ_q , τ_0 , and $[Q]$ are the SV quenching constant, quenching rate constant, decay time of the fluorophore in absence of quencher, and the concentration of free quencher, respectively. As can be seen in Figure 8, a plot of F_0/F of LH_2 versus $[\text{BSA}]$ exhibits a good linearity ($R = 0.994$) and affords K_{SV} value $2.42 \pm 0.01 \times 10^5 \text{ M}^{-1}$ at 298 K. The amplitude-weighted average lifetime in the absence of quencher, $\langle \tau \rangle_0$, can be calculated from the biexponential decay data of LH_2 in the homogeneous buffer given in Table 1 and found to be about 8.0 ns. From this data, the bimolecular quenching rate constant, κ_q , can be calculated as $3 \times 10^{13} \text{ M}^{-1} \text{ s}^{-1}$. This value is almost 3 orders of magnitude greater than the maximum diffusion-limited quenching rate constant, which is known to be of the order of $2 \times 10^{10} \text{ M}^{-1} \text{ s}^{-1}$.³⁷ Therefore, the quenching process is assumed mainly to be controlled by static quenching mechanism rather than dynamically controlled process.

For a static quenching process, K_{SV} can be regarded as the association constant (K_a) for the formation of the fluorophore–quencher complex in the ground state.³⁸ The idea of static quenching can further be supported by doing temperature variation experiment. The calculated K_a values from the linear SV plots given in Figure 8 are collected in Table 2. It is seen that the magnitude of K_a decreases with increase in temperature, which further supports the formation of a protein– LH_2 complex responsible for the fluorescence quenching. Interestingly, the K_a value in this case is about 4 orders of magnitude higher than that of LH_2 –HSA binding,¹⁸ which indicates far stronger interaction of LH_2 with BSA.

3.5.2. Thermodynamics of Ligand Binding. The binding constant values given in Table 2 at different temperature are further used to calculate the thermodynamic parameters of LH_2 –BSA interaction. If the enthalpy change (ΔH) does not vary significantly in the temperature range studied, van't Hoff relation (eq 6) can be used to evaluate the enthalpy and entropy change for LH_2 binding to BSA,³⁹ whereas the corresponding Gibbs free energy parameter is calculated from the relationship given in eq 7.

$$\log K = -\frac{\Delta H}{2.303RT} + \frac{\Delta S}{2.303R} \quad (6)$$

$$\Delta G = \Delta H - T\Delta S \quad (7)$$

All the parameters obtained from the linear van't Hoff plot (not shown) are also listed in Table 2. The negative values of ΔG assert that the binding process is spontaneous in the whole temperature range. Further, the ΔG value for LH_2 –BSA complex formation is about 3 times more than that for the LH_2 –HSA interaction, which is consistent with the assumption of more favorable binding in the former. The high negative value of ΔH in this case indicates that the binding is an enthalpy-driven process; although the positive entropy change points to the fact that the structural distortion also contributes a major part in the binding process. In contrast, the binding of LH_2 in HSA was reported to be associated with negative ΔS value.¹⁸ Overall, the present study reveals that, although BSA and HSA are structurally similar, the mechanism and consequently the thermodynamics of binding of LH_2 in these carrier proteins are distinctly different (see below).

It is to be noted here that LH_2 fluorescence quenching in the presence of HSA showed a downward curvature in SV plot and

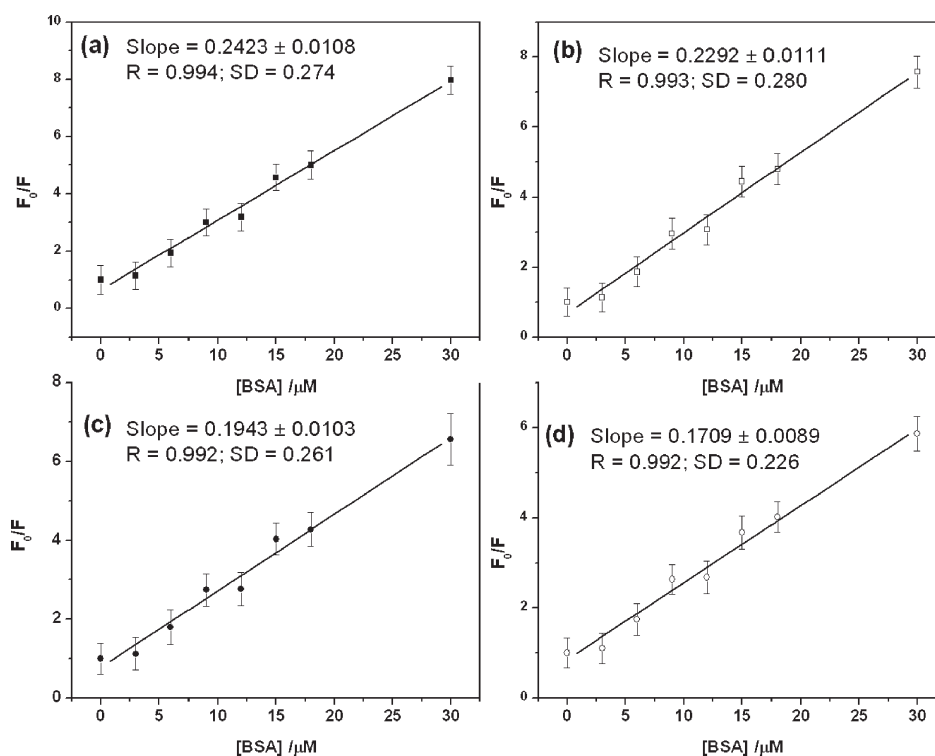


Figure 8. Stern–Volmer (SV) plots of LH₂ fluorescence quenching in presence of BSA at 298 K (a), 303 K (b), 313 K (c), and 318 K (d). The parameters obtained from linear fitting of the data using eq 5 are also shown in each case.

Table 2. Thermodynamic Parameters Corresponding to Binding of LH₂ with BSA^a

temp/K	binding const/ 10^5 M^{-1}	$\Delta H/$ kJ mol^{-1}	$\Delta S/$ $\text{J K}^{-1} \text{ mol}^{-1}$	$\Delta G/$ kJ mol^{-1}
298	2.423 ± 0.108	-13.529	57.997	-30.812
303	2.292 ± 0.111			-31.102
308	2.274 ± 0.166			-31.392
313	1.943 ± 0.103			-31.689
318	1.709 ± 0.089			-31.971

^a The binding constant values were taken from the slope of the Stern–Volmer plot. The other thermodynamic parameters were obtained using eqs 6 and 7 with an error limit of $\pm 10\%$.

was explained on the basis of fractional accessibility of the fluorophore to bind within the protein cavity.¹⁸ However, no such curvature was found with BSA in the present study. This difference can be explained on the basis of the location of the binding sites of the albumins. Although BSA is structurally homologous to HSA, the former contains an extra binding pocket (subdomain IA) which is relatively more exposed to the aqueous medium in addition to a more hydrophobic binding region in subdomain IIA for both the proteins.^{40,41} In an earlier communication, we have shown that the relatively nonpolar fraction of LH₂ binds in the hydrophobic binding region in subdomain IIA of HSA.¹⁸ However, in the case of BSA, the exposed binding region in subdomain IA is also available for the relatively more polar fraction of LH₂ in addition to the hydrophobic binding in subdomain IIA for the nonpolar fraction similar to the HSA binding. As a result, the overall fluorescence quenching follows simple SV relation.

These two binding sites in BSA can be assumed to be cooperative in nature and results in a sigmoidal decrease in fluorescence intensity with increasing quencher concentration. The strong nature of LH₂ binding is also confirmed by fluorescence spectral blue shift of ca. 6 nm in BSA compared to the bulk aqueous medium (Figure 6). On the other hand, in HSA apparently no spectral shift is observed (inset, Figure 2S in the Supporting Information). Furthermore, the relative quenching of LH₂ fluorescence intensity is almost 5 times in BSA compared to HSA under similar quencher concentration.

An important equation involved in quantitative description of cooperative binding process and analysis of the LH₂ fluorescence quenching in presence of BSA is given by the modified Hill equation:^{42,43}

$$\Delta F = \Delta F_{\max} \frac{[S]^{n_H}}{K_{0.5}^{n_H} + [S]^{n_H}} \quad (8)$$

where $\Delta F (=F_0 - F)$ is the change in fluorescence intensity in the presence of substrate concentration $[S]$ and ΔF_{\max} is the maximum change in fluorescence intensity, $K_{0.5}$ is the concentration of substrate that gives half-maximal fluorescence change, and n_H represents the Hill coefficient. The value of n_H is usually a whole number and if it is greater than 1, the situation is represented by positive cooperativity, whereas the value of n_H equal to 1 represents a situation without any cooperativity.

Figure 9 represents the simulation of LH₂–BSA data using eq 8 at different temperatures. It is evident that the experimental data points are nicely correlated and the statistical parameters are fairly acceptable with correlation coefficient greater than 0.99 in all the cases. Interestingly, the magnitude of n_H is very close to 2, indicating the positive cooperativity with involvement of both

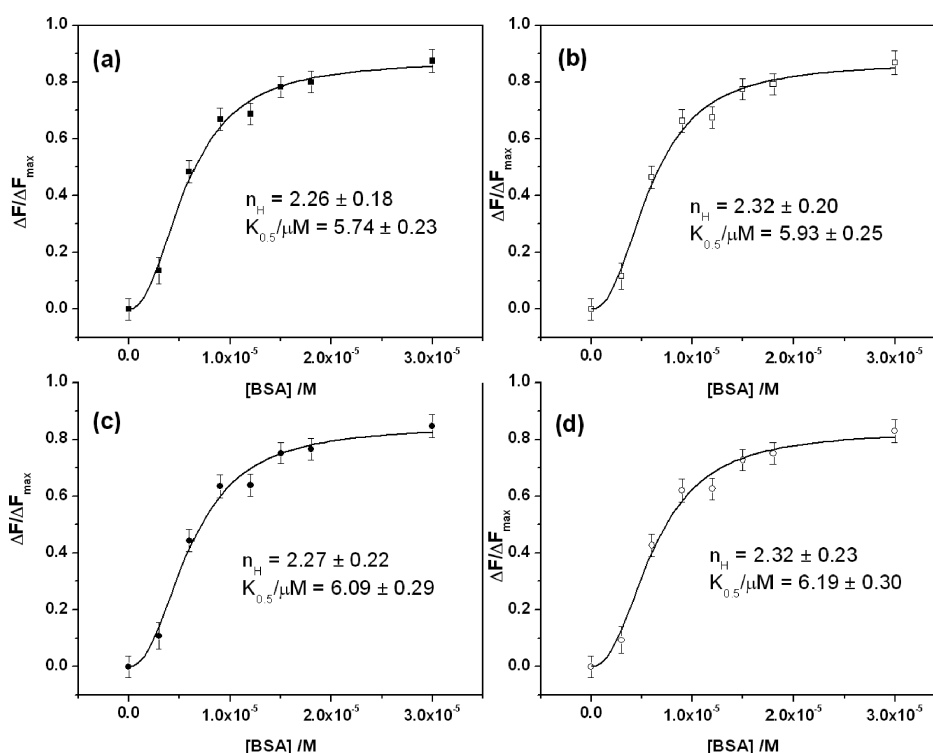


Figure 9. Hill plot for the LH₂–BSA system at 298 K (a), 303 K (b), 313 K (c), and 318 K (d). The solid line indicates the simulation of experimental data points using eq 8. The corresponding parameters obtained from the fitting result are also shown.

the binding sites in BSA. However, similar analysis in the case of HSA (Figure 4S in the Supporting Information) results in the value of n_H to be very close to 1, indicating the absence of any cooperative mechanism in this case. Initial binding of LH₂ in the more exposed ligand binding site at the surface of BSA causes a massive structural change in a cooperative manner so that the hydrophobic binding site in subdomain IIA also becomes easily accessible for LH₂ binding. This reorganization in the protein structure on ligand binding is also manifested from the overall positive change in ΔS value calculated above. Further, the cooperativity is manifested in almost 4 orders of magnitude higher value of binding constant and also about 3 times greater negative free energy change in case of BSA binding while comparing with HSA.

4. CONCLUSIONS

The excited-state photophysical behavior of luminol (LH₂) in biological media has been studied by steady-state and time-resolved fluorescence spectroscopy. The observed fluorescence quenching is due to the sequestration of the nonpolar fraction of LH₂ in hydrophobic domains. The facile association of LH₂ in CTAB micellar core is explained on the basis of dipole–dipole type of interaction between the charge-localized excited fluorophore with positive surfactant head group. Binding of LH₂ in ligand binding domains IA and IIA of BSA is thermodynamically favorable and mainly controlled by an enthalpy-driven process. However, entropy contribution into the higher negative Gibb's free energy (ΔG) stems from massive structural distortion of the protein secondary structure due to the positive cooperativity of the two binding sites in BSA in comparison with structurally homologous HSA. The recovery of fluorescence intensity in the presence of bilirubin can be used as an assay for more sensitive analytical application of LH₂ in forensic science.

■ ASSOCIATED CONTENT

S Supporting Information. Variation in intensity of fluorescence for the LH₂–CTAB system with increasing concentration of β -cyclodextrin (CD) (Figure 1S), variation of LH₂ fluorescence with increasing concentration of HSA (Figure 2S), increase in fluorescence intensity of the LH₂/BSA solution in the presence of bilirubin (BIL) (Figure 3S), and Hill plot for the LH₂–HSA system at different temperatures (Figure 4S). This material is available free of charge via the Internet at <http://pubs.acs.org>.

■ AUTHOR INFORMATION

Corresponding Author

*Phone: (91)-364-2722634. Fax: (91)-364-2550076. E-mail: smitra@nehu.ac.in, sivaprasadm@yahoo.com.

■ ACKNOWLEDGMENT

Financial support through research project 2009/37/26/BRNS from the Board of Research in Nuclear Sciences (BRNS), Government of India, is gratefully acknowledged. The authors thank Dr. A. Bhasikuttan of Bhaba Atomic Research Center (BARC) for helpful discussion. Thanks are also due to AIRF, JNU, for their help in TCSPC measurement.

■ REFERENCES

- (1) Kricka, K. J. *Anal. Chem.* **1995**, *67*, 499–502.
- (2) Yeshion, T. E. In *Bioluminescence and Chemiluminescence: Current Status*; Stanley, P. E., Kricka, K. J., Eds.; John Wiley: New York, 1991; p 379.
- (3) Bowie, A. R.; Sanders, M. G.; Worsfold, P. J. *J. Biolumin. Chemilumin.* **1996**, *11*, 61–90.

- (4) Budavari, S., Ed.; *The Merck Index*, 12th ed.; Merck & Co., Inc.: Whitehall, NJ, 1996; p 957.
- (5) Wu, Y.; Zhuang, Y.; Liu, S.; He, L. *Anal. Chim. Acta* **2008**, *630*, 186–193.
- (6) Zhang, H.; Shibata, T.; Krawczyk, T.; Kabashima, T.; Lu, J.; Lee, M. K.; Kai, M. *Talanta* **2009**, *79*, 700–705.
- (7) Bi, S.; Zhou, H.; Zhang, S. *Biosens. Bioelectron.* **2009**, *24*, 2961–2966.
- (8) Kahl, R.; Weimann, S.; Weinke, S.; Hilderbrandt, A. G. *Arch. Toxicol.* **1987**, *60*, 158–162.
- (9) Irie, S. *Curr. Ther. Res.* **1960**, *2*, 132–136.
- (10) Irie, S. *Curr. Ther. Res.* **1960**, *2*, 107–110.
- (11) Irie, S. *Curr. Ther. Res.* **1960**, *2*, 153–157.
- (12) Larkin, T.; Gannicliffe, C. *Sci. Justice* **2008**, *48*, 71–75.
- (13) Lasovsky, L.; Grambal, F. *Bioelectrochem. Bioenerg.* **1986**, *15*, 95–102.
- (14) Voicescu, M.; Vesilescu, M.; Constantinescu, T.; Meghea, A. *J. Lumin.* **2002**, *97*, 60–67.
- (15) Seitz, W. R. *J. Phys. Chem.* **1975**, *79*, 101–106.
- (16) Komatsu, T.; Ohira, M.; Yamada, M.; Suzuki, S. *Bull. Chem. Soc. Jpn.* **1986**, *59*, 1849–1855.
- (17) Moyon, N. S.; Chandra, A. K.; Mitra, S. *J. Phys. Chem. A* **2010**, *114*, 60–67.
- (18) Moyon, N. S.; Mitra, S. *Chem. Phys. Lett.* **2010**, *498*, 178–183.
- (19) He, X. M.; Carter, D. C. *Nature* **1992**, *358*, 209–215.
- (20) Kohn, E. J. *Chem. Rev.* **1941**, *28*, 395–417.
- (21) Olson, R. E.; Christ, D. D. *Annu. Rep. Med. Chem.* **1996**, *31*, 327–336.
- (22) Valeur, B. In *Molecular Fluorescence Principles and Applications*; Wiley-VCH: Weinheim, FRG, 2002.
- (23) Meech, S. R.; Phillips, D. J. *Photochem.* **1983**, *23*, 193–217.
- (24) Mataga, N.; Kubota, T. In *Molecular interactions and electronic spectra*; Marcel Dekker Inc.: New York, 1970.
- (25) Bevington, P. R. In *Data reduction and error analysis for the physical sciences*; McGraw-Hill, Inc.: New York, 1969.
- (26) Das, S. K.; Bansal, A.; Dogra, S. K. *Bull. Chem. Soc. Jpn.* **1997**, *70*, 307–313.
- (27) Barnadas-Rodriguez, R.; Estelrich, J. *J. Phys. Chem. B* **2009**, *113*, 1972–1982.
- (28) Szejtli, J. In *Controlled drug bioavailability*; Smolen, V., Ball, L. A., Eds.; Wiley: New York, 1985; pp 365–420.
- (29) Matsushita, Y.; Suzuki, T.; Ichimura, T.; Hikida, T. *J. Phys. Chem. A* **2004**, *108*, 7490–7496.
- (30) Karatani, H. *Chem. Lett.* **1986**, 377–380.
- (31) Maeztu, R.; Tardajos, G.; Gonzalez-Gaitano, G. *J. Phys. Chem. B* **2010**, *114*, 2798–2806.
- (32) Maeztu, R.; Gonzalez-Gaitano, G.; Tardajos, G. *J. Phys. Chem. B* **2010**, *114*, 10541–10549.
- (33) Ogino, H. *J. Am. Chem. Soc.* **1981**, *103*, 1303–1304.
- (34) Wylie, R. S.; Macartney, D. H. *J. Am. Chem. Soc.* **1992**, *114*, 3136–3138.
- (35) Connors, K. A. *Binding Constants. The Measurements of Molecular Complex Stability*; Wiley: New York, 1987.
- (36) Peterson, C. E.; Ha, C.-E.; Harohalli, K.; Feix, J. B.; Bhagavan, N. V. *J. Biol. Chem.* **2000**, *275*, 20985–20995.
- (37) Ware, W. R. *J. Phys. Chem.* **1962**, *66*, 455–458.
- (38) Lakowicz, J. R. In *Principles of fluorescence spectroscopy*, 3rd ed.; Springer: Singapore, 2006; p 282.
- (39) Silbey, R. J.; Alberty, R. A. In *Physical Chemistry*, 3rd ed.; John Wiley & Sons (Asia) Pte. Ltd.: Singapore, 2002.
- (40) (a) Carter, D. C.; He, X. M. *Science* **1990**, *249*, 302–303. (b) He, X. M.; Carter, D. C. *Nature* **1992**, *358*, 209–215. (c) Dockal, M.; Carter, D. C.; Ruker, F. *J. Biol. Chem.* **1999**, *274*, 29303–29310. (d) Carter, D. C.; Ho, J. X. *Adv. Protein Chem.* **1994**, *45*, 153–203.
- (41) (a) Sudlow, G.; Birkett, D. J.; Wade, D. N. *Mol. Pharmacol.* **1975**, *11*, 824–832. (b) Sudlow, G.; Birkett, D. J.; Wade, D. N. *Mol. Pharmacol.* **1976**, *12*, 1052–1061. (c) Zhong, D.; Douhal, A.; Zewail, A. H. *Proc. Natl. Acad. Sci. U.S.A.* **2000**, *97*, 14056–14061. (d) Chuang, V. T. G.; Otagari, M. *Chirality* **2006**, *18*, 159–166.
- (42) Chatterjee, T.; Mukherjee, D.; Dey, S.; Pal, A.; Hoque, K. M.; Chakrabarti, P. *Biochemistry* **2011**, *50*, 2962–2972.
- (43) Pratap, P. R.; Mikhaylyants, L. O.; Olden-Stahl, N. *Biochim. Biophys. Acta* **2009**, *1794*, 1549–1557.